

# Mesoporous Copper–Magnesium Oxide Hybrid Nanocatalyzed Synthesis of 3-Substituted Isocoumarins from 2-Iodobenzoic Acid and Terminal Alkyne under Green Conditions

Manish Rawat and Diwan S. Rawat\*

Cite This: *ACS Omega* 2023, 8, 16263–16272

Read Online

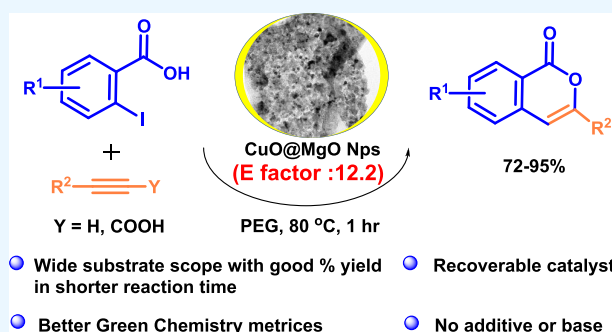
ACCESS |

Metrics &amp; More

Article Recommendations

Supporting Information

**ABSTRACT:** A 3-substituted isocoumarin scaffold has captivated extensive interest in synthetic and medicinal chemistry due to its presence in various natural products with diverse biological activities. Herein, we report a mesoporous CuO@MgO nanocomposite that was prepared *via* the sugar-blowing induced confined method with an *E*-factor of 12.2 and its catalytic potential in the facile synthesis of 3-substituted isocoumarin from 2-iodobenzoic acids and terminal alkynes. Powder X-ray diffraction, scanning electron microscopy, high-resolution transmission electron microscopy, energy-dispersive X-ray analysis, X-ray photoelectron spectroscopy, and Brunauer–Emmett–Teller techniques were utilized for the characterization of the as-prepared nanocomposite. A broad substrate scope, mild reaction conditions, excellent yield in short reaction time, no usage of additives, and better green chemistry metrics such as a low *E*-factor (0.71), high reaction mass efficiency (58.28%), low process mass efficiency (1.71), and high turnover number (629) are the various advantages of the present synthetic route. The nanocatalyst was recycled and reused up to five runs without significant loss in its catalytic activity and a very low leaching of copper (3.20 ppm) and magnesium ions (0.72 ppm). Powder X-ray diffraction and high-resolution transmission electron microscopy techniques confirmed the structural integrity of the recycled CuO@MgO nanocomposite.



## INTRODUCTION

Porous materials have been extensively explored in sensing, drug discovery, gas storage, heterogeneous catalyst, etc.<sup>1</sup> A well-defined pore size and shape provide the distinct adsorption sites to porous materials, whereas particle aggregation can be prevented by the pore size.<sup>2</sup> The slight difference in pore size of microporous and mesoporous materials stimulated the diffusion, resettling, and activation of reactants in the pore of mesoporous materials.<sup>3</sup> The mesoporous materials have been widely explored in the field of drug delivery, adsorption, sensors, catalysis, etc., due to their high surface area and adjustable pore topology.<sup>4–7</sup> The potential utilization of mesoporous materials as the support for the nanoparticle depends upon the pore topology of mesoporous materials with confined pore size distribution.<sup>8</sup> Mesoporous metal oxides such as TiO<sub>2</sub>,<sup>9</sup> Al<sub>2</sub>O<sub>3</sub>,<sup>10</sup> SiO<sub>2</sub>,<sup>11</sup> ZrO<sub>2</sub>,<sup>12</sup> CeO<sub>2</sub>,<sup>12</sup> Fe<sub>2</sub>O<sub>3</sub>,<sup>13</sup> MgO,<sup>14</sup> etc., have been extensively reported as the catalyst support. MgO provides numerous advantages over other metal oxides as it possesses unique Lewis acid–base bifunctional activities, eco-friendly properties, being less expensive, irreducible oxide, and lower environmental effects in accordance with the clean water act basic limits.<sup>15,16</sup> The existence of several edge corner defect sites with Lewis acidic Mg<sup>+2</sup> and Lewis basic O<sup>-2</sup> sites

accompanying with several crystal defects make MgO as the better option for the nanoparticle support. These exposed sites facilitate the progress of reaction in shorter time.<sup>17</sup> MgO has been extensively explored as the nanoparticle support for several transformations such as nitro reductions using Au/MgO,<sup>18</sup> oxidative dehydrogenation using V<sub>2</sub>O<sub>5</sub>/MgO,<sup>19</sup> CO<sub>2</sub> reforming of methane using Ni/MgO,<sup>20</sup> and so on.

The implementation of copper-based nanomaterials as a robust heterogeneous catalyst on a variety of organic transformations has garnered notable attention due to their cost-effectiveness, low toxicity, and easy accessibility of Cu<sup>0</sup>, Cu<sup>I</sup>, Cu<sup>II</sup>, and Cu<sup>III</sup> oxidation states owing to their reactivity *via* one-electron and two-electron reaction pathways.<sup>21</sup> Different oxidation states of copper enable the activation of diverse functional groups through Lewis acid interactions or  $\pi$ -coordination.<sup>22</sup> One of the cost-effective strategies of constructing the advanced and robust copper-based nano-

Received: February 2, 2023

Accepted: April 12, 2023

Published: April 24, 2023



particles for catalysis is to stabilize copper nanoparticles over other types of support to suppress the agglomeration of copper nanoparticles.<sup>21</sup> Various methods have been reported for the synthesis of copper-based nanocomposites such as electrochemical, chemical, and biogenic methods. One of the green approaches is the biogenic method, which involves natural reducing agents such as enzymes, plant extracts, and microorganisms.<sup>23</sup> Transition metal-based nanoparticles have been explored as a highly active and selective catalyst for numerous synthetic methodologies. The improved catalytic properties of nanoparticles are often credited to their enhanced surface area to volume ratio along with size-dependent changes in their electronic structure, which allows the charge distribution in electron-transfer processes.<sup>24</sup>

Isocoumarins are the core moiety of numerous natural products.<sup>25–27</sup> They exhibit multifarious pharmacological activities such as antifungal,<sup>28</sup> antimicrobial,<sup>29</sup> anti-HIV,<sup>30</sup> antidiabetic,<sup>31</sup> antitumor,<sup>32</sup> and anti-inflammatory.<sup>33</sup> Some of the 3-substituted isocoumarins possessing biological activities are shown in Figure 1. Aside from these activities, they also are

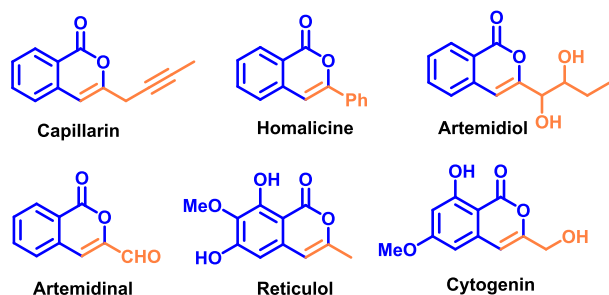
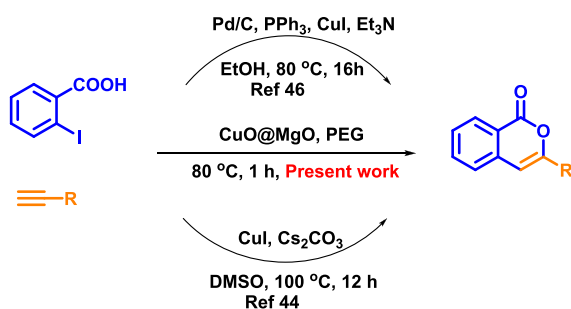


**Figure 1.** Representative examples of 3-substituted coumarins containing pharmacological properties.

used as a synthons for the synthesis of important heterocycles like isochromenes, isoquinolines, isocarbostyrils, and 3,4-dihydroisocoumarins.<sup>34–38</sup> The biological importance of 3-substituted isocoumarins has led to develop the notable synthetic methodologies for the formation of this scaffold *via* transition metal catalyzed reactions.<sup>39–43</sup>

Among all, one of the most efficient protocols for the formation of isocoumarins is 6-*endo dig* cyclization of 2-alkynylbenzoic acid or esters using palladium, copper, silver, and Lewis acid catalyst.<sup>44–49</sup> These approaches display some restrictions such as the non-recyclable catalytic system, usage of additives or bases, toxic organic solvents, higher reaction time, high temperature, and regioselectivity problem (Scheme 1).

### Scheme 1. Catalysis for the Synthesis of 3-Substituted Coumarins from 2-Iodobenzoic Acid and Terminal Alkyne



There is a necessity of an efficient recyclable nanocatalyst for the synthesis of isocoumarins under mild reaction conditions. Keeping these foregoing concerns in mind and in continuation of our efforts toward the area of nanocatalysis,<sup>50–53</sup> herein, we report the development of the recyclable mesoporous CuO@MgO nanocomposite system for the synthesis of 3-substituted isocoumarins from 2-iodobenzoic acid and terminal alkyne *via* Sonogashira-type coupling reaction followed by 6-*endo-dig* cyclization with better green chemistry metrics.

## RESULTS AND DISCUSSION

**Synthesis and Characterization of CuO@MgO Nanocomposites.** The CuO@MgO nanocomposites were synthesized using the sugar-blowing induced confined synthesis method.<sup>54</sup> Transparent solution containing copper nitrate, magnesium nitrate, and glucose was heated at 100 °C for 12 h for complete evaporation results in a gel-like black solid. Then, the calcination of this gel-like black solid Cu(NO<sub>3</sub>)<sub>2</sub>·Mg(NO<sub>3</sub>)<sub>2</sub>·glucose mixture was performed at 550 °C for 3 h, resulting in CuO@MgO nanocomposites (Scheme 2).

The powder X-ray diffraction of the CuO@MgO nanocatalyst revealed the deposition of monoclinic CuO over the cubic MgO. The phases (−110), (002), (111), (−202), (020), (113), (−311), (220), and (311) correspond to peaks at 32.4, 35.44, 38.66, 48.69, 53.45, 58.21, 66.13, 68.05, and 72.31°, respectively, of CuO (JCPDS 45-0937), whereas the phases (111), (200), (220), (311), and (222) correspond to peaks at 36.68, 42.85, 61.52, 75.11, and 78.60°, respectively, of MgO (JCPDS 45-0946). The particle size was found to be 17.43 nm using the Scherrer formula (Figure 2). The surface morphology of the CuO@MgO nanocomposite was analyzed and characterized using scanning electron microscopy (SEM), as shown in Figure 3. The SEM results reveal the loading of copper oxide over honeycomb-like magnesium oxide.

Figure 4a–e shows high-resolution transmission electron microscopy (HR-TEM) images, which reveals that the black copper oxide nanoparticles are well embedded over MgO nanosheets. Figure 4f shows the selected area electron diffraction (SAED) pattern in which diffraction rings correspond to the (002) and (113) planes of CuO and (200) and (311) planes of MgO.

The energy-dispersive X-ray analysis (EDAX) elemental analysis of CuO@MgO nanocomposites indicated the presence of 28.6, 28.3, and 31.9 wt % of copper, magnesium, and oxygen, respectively, as shown in Figure 5.

XPS analysis was examined for confirmation of surface distribution and elemental state of CuO@MgO nanocomposites. Figure 6 shows the high-resolution spectra of Cu 2p, Mg 2p, and O 1s.

The binding energies situated at 932.1 and 952.1 eV correspond to 2p<sub>3/2</sub> and 2p<sub>1/2</sub> orbitals of Cu<sup>2+</sup> with satellite peaks located at 940.4 and 960.2 eV, respectively. The difference in binding energies of Cu 2p<sub>3/2</sub> and Cu 2p<sub>1/2</sub> is 20 eV, which is characteristic for the existence of CuO.<sup>53,55</sup> The high-resolution spectrum of Mg 2p shows a peak at 47.6 eV, whereas two peaks allocated at 85.7 and 86.8 eV are observed for Mg 2s, which can be associated with Mg–OH and Mg–O linkages, respectively. The peak observed in the O 1s spectrum at 529.1 eV corresponds to the O–Mg band, which revealed the presence of MgO.<sup>54,56</sup>

Next, we investigated the nitrogen adsorption/desorption isotherm and pore diameter of CuO@MgO, as shown in Figure 7. It is assigned to the isotherm with a type H3

## Scheme 2. Preparation of CuO@MgO Nanocomposites

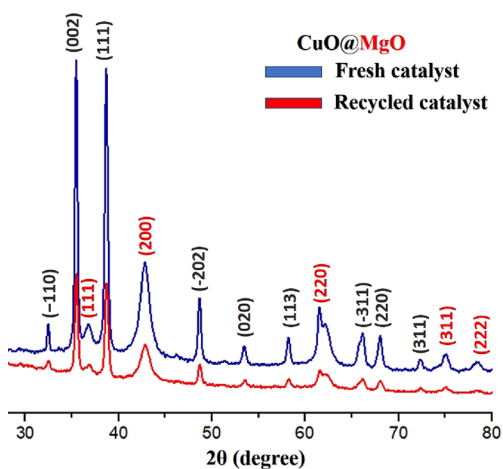
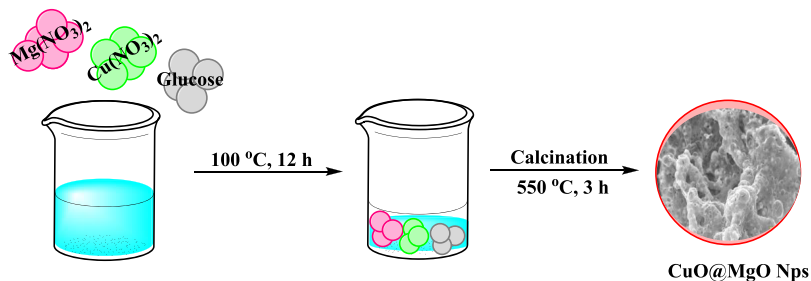


Figure 2. PXRD of the CuO@MgO nanocatalyst.

hysteresis loop. The nanocomposite CuO@MgO has a pore size of 29.012 Å (calculated from the adsorption branch by the Barrett–Joyner–Halenda (BJH) model), BET (Brunauer–Emmett–Teller) surface area of 60.935 m<sup>2</sup>/g, pore diameter of 29.012 Å, and a pore volume of 0.158 cm<sup>3</sup>/g.

**CuO@MgO Nanocomposite Catalyzed Synthesis of Isocoumarin Derivatives.** The catalytic evaluation of the

CuO@MgO nanocomposite was explored for the synthesis of isocoumarin with a wide substrate scope. A model reaction between 2-iodobenzoic acid **1** and phenylacetylene **2** using the CuO@MgO nanocatalyst in various solvents or neat conditions at 80 °C was performed for the optimization study, as shown in Table 1. Polar solvents like acetonitrile, DMF, and DMSO are favorable to furnish the desired product in 70, 82, and 78% yields, respectively (Table 1, entries 1–3). No desired product was observed in the case of non-polar solvent toluene (Table 1, entry 4). Then, green solvents like ethanol, water, EG, PEG, and neat conditions were screened, and it was found that ethanol, water, and neat conditions have no contribution in product formation even after a longer time period (Table 1, entries 5–7) whereas ethylene glycol and polyethylene glycol are favorable solvents for the CuO@MgO nanocatalyst with 76 and 92%, respectively (Table 1, entries 8 and 9). The rise in temperature does not display further enhancement in the progress of reaction, whereas the fall in temperature decreased the % yield from 92 to 62% in 12 h (Table 1, entries 10 and 11). Next, we screened the amount of catalyst loading, and the decrease and increase in the amount of catalyst led to lowering and no change in % yield of the desired product (Table 1, entries 12 and 13). The catalytic property of CuO@MgO was compared with some commonly supported copper nanoparticles such as CuO@SiO<sub>2</sub> and

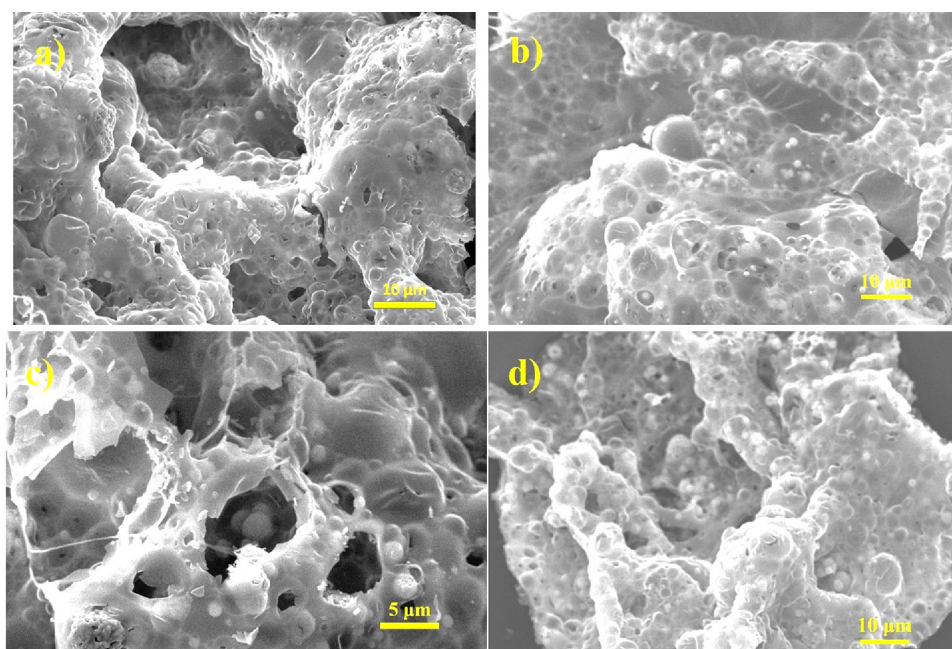


Figure 3. (a–d) SEM images of the CuO@MgO nanocatalyst at different magnifications.

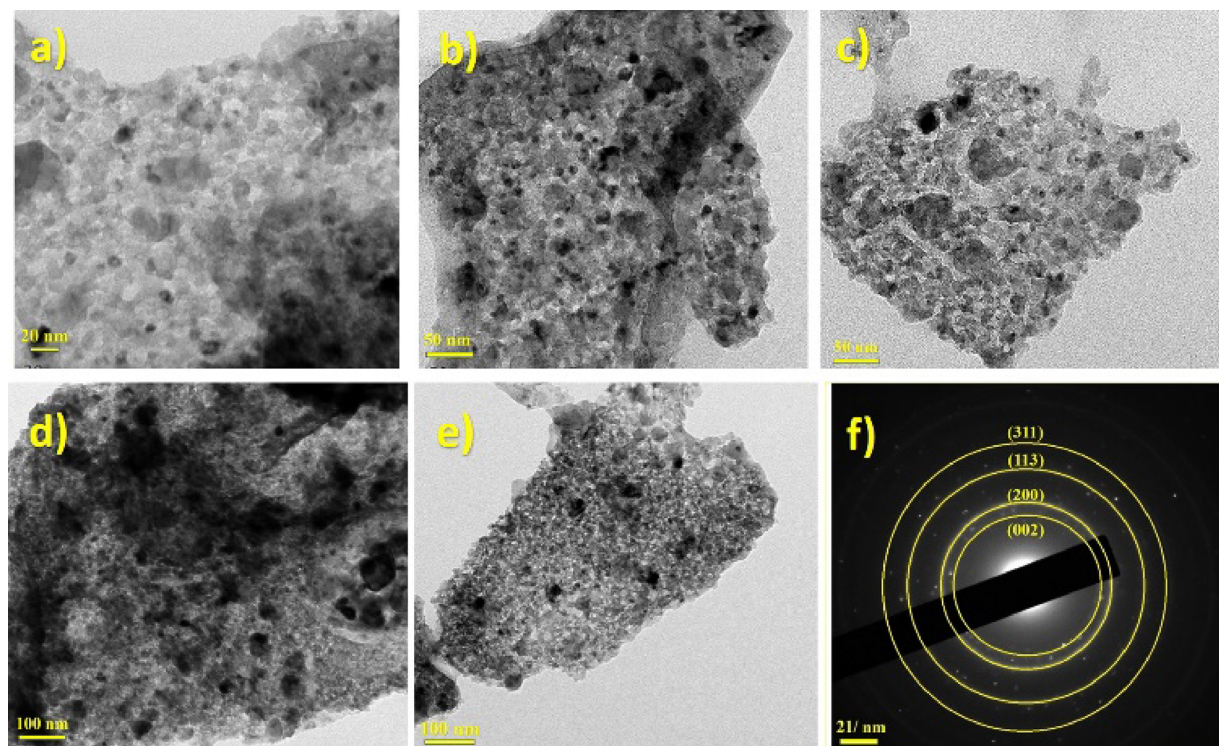


Figure 4. (a–e) HR-TEM images; (f) SAED image of CuO@MgO nanocomposites.

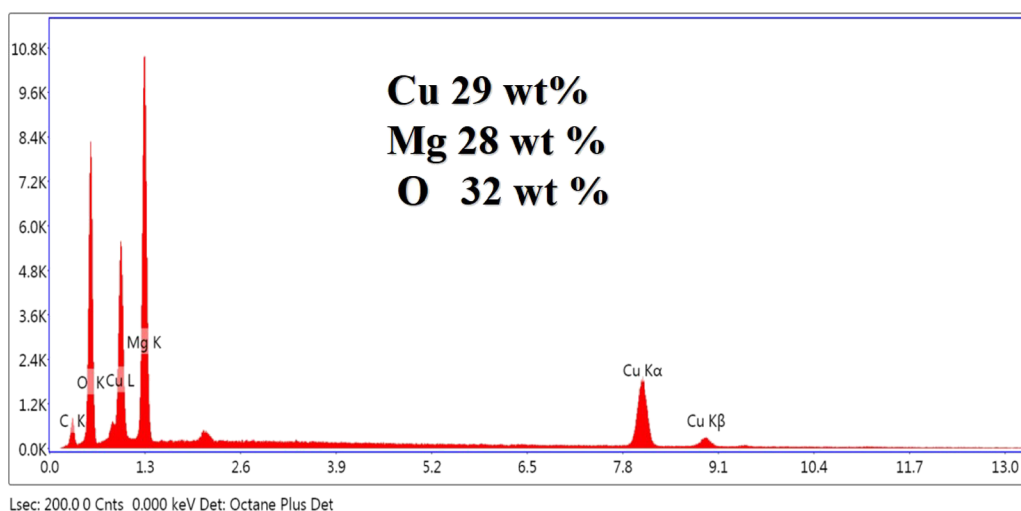


Figure 5. EDAX analysis of CuO@MgO nanocomposites.

CuO@Al<sub>2</sub>O<sub>3</sub>. It was evaluated that the present catalytic nanohybrid is best suitable for the reaction compared to the other two (Table 1, entries 14 and 15). Then, both the components of the nanohybrid were used as the catalyst for the reaction and the results clearly indicated that the CuO@MgO nanohybrid is the most suited catalyst for reaction as compared to both the components (Table 1, entries 16 and 17). In summary, the synthesis of 3-substituted isocoumarins from 2-iodobenzoic acid and terminal alkyne was efficiently catalyzed by the CuO@MgO nanohybrid at 80 °C in the PEG solvent.

The generality of the present methodology using the CuO@MgO nanocatalytic system under optimized conditions was examined by various electron donating and withdrawing substituents on 2-iodobenzoic acid and alkyne substrates, as shown in Table 2. Initially, different alkynes were screened; it

was observed that the reaction proceeded smoothly with particularly good % yield with phenyl acetylene and derivative having the electron donating group (–CH<sub>3</sub>) (Table 2, entries 3a and 3b), whereas a slight drop in % yield was observed in the case of the derivative bearing electron withdrawing group (–F) (Table 2, entry 3c). Then, aliphatic alkynes like but-2-ynoic acid, pentyne, and octyne were evaluated and gave the corresponding products in excellent % yield (Table 2, entries 3d, 3e, and 3f).

It is worth mentioning that alkyl alkynes like 3-methoxyprop-1-yne and hex-5-ynenitrile bearing the valuable functionalities such as OMe and CN could be transformed into the desired product in particularly good % yield (Table 2, entries 3g and 3h). Cyclic alkyne like ethynylcyclopropane proceeded well under optimal conditions with the correspond-

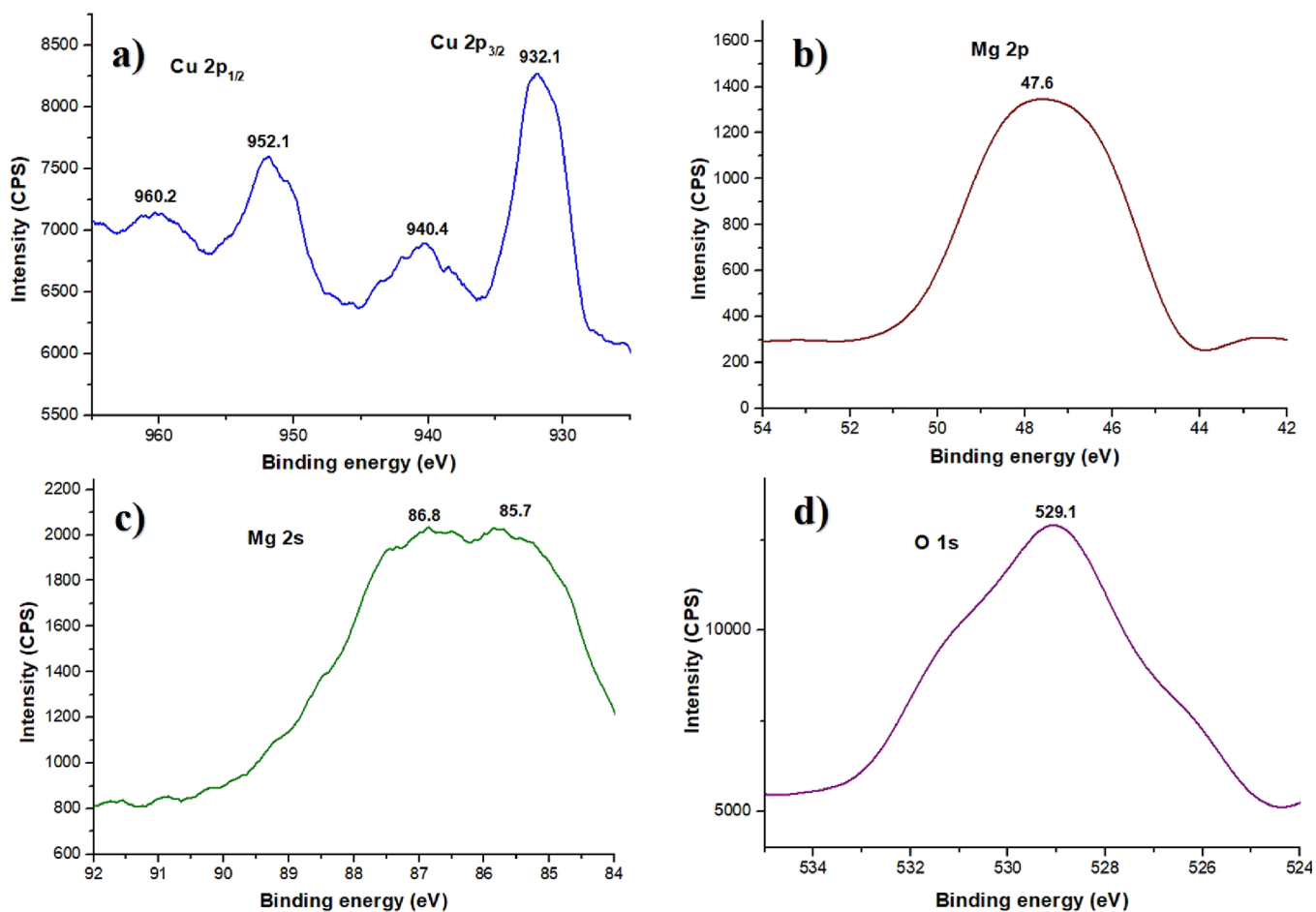


Figure 6. (a–d) High-resolution XPS spectra of CuO@MgO nanocomposites.

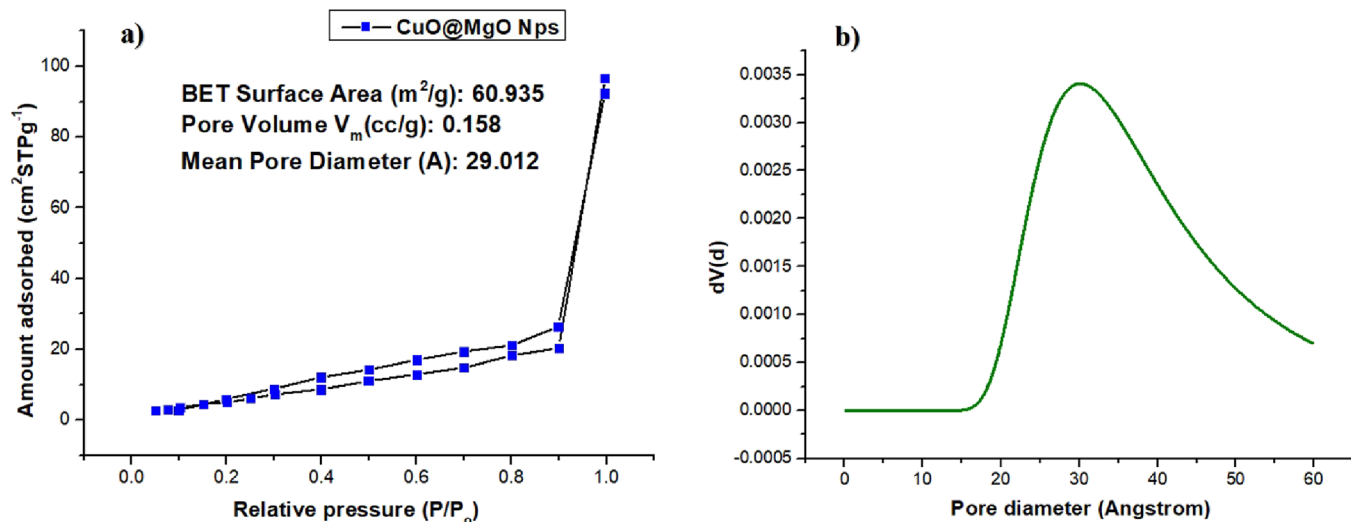


Figure 7. (a) Nitrogen adsorption–desorption isotherms; (b) pore diameter of the CuO@MgO nanocomposite.

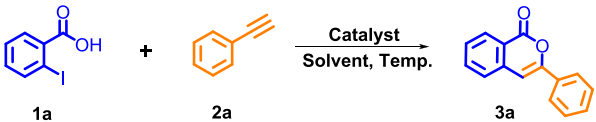
ing product in good 78% yield (Table 2, entry 3i). Next, we explored the compatibility of various 2-iodobenzoic acids, and it was found that methyl, bromo, and pyridyl groups were well tolerated with excellent to good % yield of the desired product (Table 2, entries 3j–3o).

The plausible mechanism of the CuO@MgO nanoparticle catalyzed the synthesis of isocoumarins, as depicted in Figure 8. Initially, the CuO@MgO nanocatalyst activates the alkyne

(2) as well as 2-iodobenzoic acid (1), leading to the formation of intermediate I *via* reductive elimination. Then, intermediate I, which is *o*-alkynyl benzoic acid, undergoes intramolecular cyclization that leads to the formation of product 3.

The recyclability of CuO@MgO was studied on a 4 mmol reaction scale over five runs under optimized conditions (Figure 9). A non-significant change in catalytic efficiency of the CuO@MgO nanocatalyst was observed after five runs.

**Table 1. Optimization of the CuO@MgO Nanohybrid Catalyzed Synthesis of 3-Substituted Isocoumarins Using 2-Iodobenzoic Acid (1a) and Terminal Alkyne (2a)<sup>a</sup>**



entry	catalyst	solvent	temp (°C)	time (h)	yield (%) <sup>b</sup>
1	CuO@MgO	ACN	80	1	70
2	CuO@MgO	DMF	80	1	82
3	CuO@MgO	DMSO	80	1	78
4	CuO@MgO	toluene	80	24	
5	CuO@MgO	EtOH	80	24	
6	CuO@MgO	water	80	24	
7	CuO@MgO	neat	80	24	
8	CuO@MgO	EG	80	1	76
9	CuO@MgO	PEG	80	1	92
10	CuO@MgO	PEG	110	1	92
11	CuO@MgO	PEG	60	12	62
12 <sup>c</sup>	CuO@MgO	PEG	80	3	76
13 <sup>d</sup>	CuO@MgO	PEG	80	1	92
14	CuO@SiO <sub>2</sub>	EG	80	5	72
15	CuO@Al <sub>2</sub> O <sub>3</sub>	EG	80	5	78
16	CuO	PEG	80	5	62
17	MgO	EG	80	24	

<sup>a</sup>Reaction conditions: 2-iodobenzoic acid **1a** (0.5 mmol), terminal alkyne **2** (0.5 mmol), CuO@MgO (10 mg), and solvent (2 mL) were stirred at appropriate temperature. <sup>b</sup>Isolated yield. <sup>c</sup>Catalyst: 5 mg was used. <sup>d</sup>Catalyst: 20 mg was used.

Powder XRD and TEM images of the recycled catalyst after the fifth run disclosed the structural integrity of the CuO@

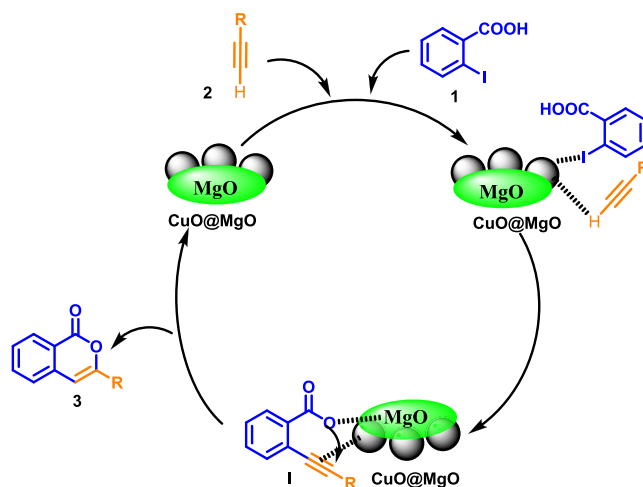
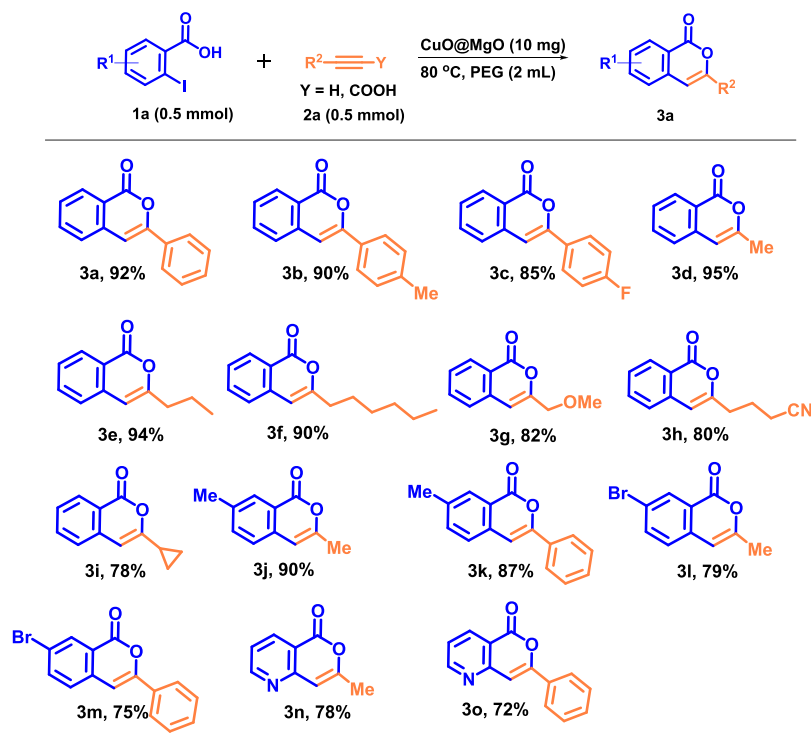


**Figure 8.** Plausible mechanism for the CuO@MgO catalyzed synthesis of isocoumarin.

MgO nanocatalyst. Then, heterogeneity of the nanocomposite was analyzed under optimized reaction conditions using the hot filtration test. Summarily, after 30 min, the reaction was stopped to 50% reaction completion. The nanocatalyst was recovered, and reaction was prolonged for 3 h at 80 °C. No further progress of reaction was observed by TLC chromatography and confirmed by <sup>1</sup>H NMR. The ICP-AES analysis of the reaction mixture detected an extremely low leached concentration of copper (3.20 ppm) and magnesium ions (0.72 ppm), which are far below the tolerance limit of the respective ions.<sup>57</sup>

Next, values of green chemistry metrics are evaluated to estimate the waste production for the synthesis of isocoumarin

**Table 2. CuO@MgO Nanocomposite Catalyzed Synthesis of Isocoumarins Using 2-Iodobenzoic Acid (1a) and Alkyne (2a)**



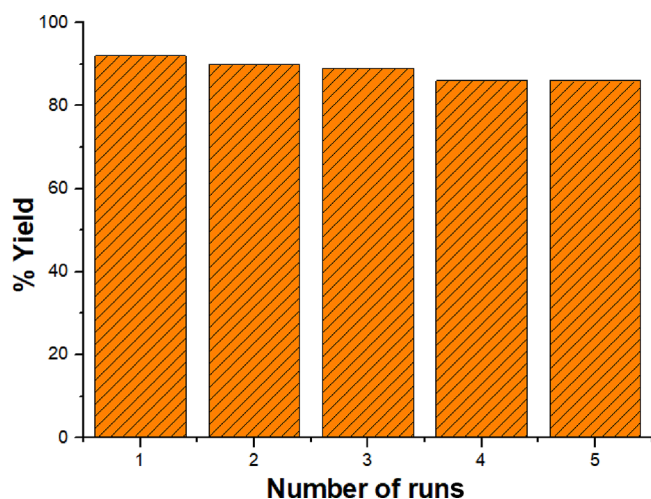


**Figure 9.** Recyclability of the CuO@MgO nanocomposite for the synthesis of compound 3a.

3a using the CuO@MgO nanocatalyst (detailed calculation in the Supporting Information). We found that the green chemistry values for the CuO@MgO nanocatalysis system are much better than the reported homogeneous catalyst (Table 3).

**Table 3. Green Chemistry Metrics**

S. no.	catalyst	<i>E</i> -factor	process mass intensity (PMI)	reaction mass efficiency (RME)	carbon efficiency (CE)
1	CuO@MgO	0.71	1.71	58.28%	92%
2	CuI/Cs <sub>2</sub> CO <sub>3</sub> (literature) <sup>44</sup>	27.82	28.82	52.29%	80.69%
3	CuI/K <sub>2</sub> CO <sub>3</sub> (literature) <sup>49</sup>	2.98	3.98	47.71%	75%

***E*-Factor of Catalyst Preparation and Organic Conversion.** To examine the sustainability and environmental impact of the present protocol, we calculated the *E*-factor for CuO@MgO nanocomposites. The *E*-factor defines as the ratio of the desired product to the total raw materials such as starting materials and solvents except water. The *E*-factor for the synthesis of the CuO@MgO nanocomposite was 12.2 (Table 4).

**Table 4. *E*-Factor Calculation for the CuO@MgO Nanocatalyst**

compounds	amount used (g)	amount recovered (g)	effective input mass (g)
Reagents ( <i>R</i> )			
Mg(NO <sub>3</sub> ) <sub>2</sub> ·6H <sub>2</sub> O	2.5	0	2.5
Cu(NO <sub>3</sub> ) <sub>2</sub> ·3H <sub>2</sub> O	1.2	0	1.2
glucose	3.6	0	3.6
total			7.3
Product			
CuO@MgO			0.6
<i>E</i> -factor	(R + S)/(prod) = 7.3/0.6		12.2

## CONCLUSIONS

In conclusion, we developed a CuO@MgO catalytic system via the sugar-blowing induced confined synthetic approach with an *E*-factor of 12.2. The catalytic capability of the CuO@MgO nanocomposite was explored for the synthesis of isocoumarins by reaction between 2-iodobenzoic acids and terminal alkynes without any base or additive in the polyethylene glycol solvent. The nanocatalyst was recycled and reused up to five runs without an appreciable loss in its catalytic activity, which was confirmed by powder XRD and TEM images. The recoverable and reusable nanocatalyst system and recyclable solvent evade the use of any additive or base, and better value green chemistry metrics such as a low *E*-factor (0.71), high reaction mass efficiency (58.28%), low process mass efficiency (1.71), and high turnover number (629) than the reported methods are diverse assets of the present synthetic protocol.

## EXPERIMENTAL SECTION

**Synthesis of CuO@MgO Nanocomposites.** CuO@MgO nanocomposites were prepared by using the modified literature method.<sup>54</sup> In a typical experimental process, Mg(NO<sub>3</sub>)<sub>2</sub>·6H<sub>2</sub>O (0.005 mol), Cu(NO<sub>3</sub>)<sub>2</sub>·6H<sub>2</sub>O (0.005 mol), and glucose (0.01 mol) were dissolved into 25 mL of water. The mixture was placed in an oven at 100 °C until complete evaporation of water to get a black gel. Then, this black gel was calcinated at 550 °C for 3 h to obtained black solid CuO@MgO nanocomposites.

**Procedure for the Synthesis of 3-Phenyl-1*H*-isochromen-1-one (3a).** A mixture of 2-iodobenzoic acid (0.5 mmol), phenylacetylene (0.5 mmol), and CuO@MgO nanoparticles (10 mg) was mixed in polyethylene glycol and stirred at 80 °C for 1 h. After the complete consumption of the reactant confirmed by thin layer chromatography, the catalyst was separated by centrifugation. Ethanol was used for washing the recovered nanocatalyst six times, and finally, the catalyst was dried in an oven. The organic layer was concentrated under reduced pressure to afford the reaction mixture. Column chromatography was used to purify the product.

**Spectral Data of Compounds.** **3-Phenyl-1*H*-isochromen-1-one (3a).** White solid; yield: 102 mg (92%); mp = 80–82 °C (lit. mp = 89–91 °C); <sup>1</sup>H NMR (CDCl<sub>3</sub>, 400 MHz) δ: 8.32 (d, *J* = 8.25 Hz, 1H), 7.91–7.89 (m, 2H), 7.75–7.71 (m, 1H), 7.53–7.42 (m, 5H), 6.97 (s, 1H); <sup>13</sup>C NMR (CDCl<sub>3</sub>, 100 MHz) δ: 162.31, 153.63, 137.52, 134.87, 131.96, 129.97, 129.65, 128.83, 128.15, 125.98, 125.25, 120.54, 101.82; HRMS (ESI-MS) (*m/z*) calcd for C<sub>15</sub>H<sub>11</sub>O<sub>2</sub>: 223.0759; found 223.0760 (M + H)<sup>+</sup>.<sup>42</sup>

**3-(*p*-Tolyl)-1*H*-isochromen-1-one (3b).** White solid; yield: 106 mg (90%); mp = 110–112 °C (lit. mp = 118–120 °C); <sup>1</sup>H NMR (CDCl<sub>3</sub>, 400 MHz) δ: 8.32 (d, *J* = 8.00 Hz, 1H), 7.80 (d, *J* = 8.25 Hz, 2H), 7.75–7.71 (m, 1H), 7.52–7.48 (m, 2H), 7.29 (d, *J* = 6.50 Hz, 2H), 6.93 (s, 1H), 2.43 (s, 3H); <sup>13</sup>C NMR (CDCl<sub>3</sub>, 100 MHz) δ: 162.44, 153.86, 140.28, 137.73, 134.82, 129.65, 129.55, 129.21, 127.91, 125.83, 125.19, 120.45, 101.08, 21.41; HRMS (ESI-MS) (*m/z*) calcd for C<sub>16</sub>H<sub>13</sub>O<sub>2</sub>: 237.0916; found 237.0925 (M + H)<sup>+</sup>.<sup>42</sup>

**3-(4-Fluorophenyl)-1*H*-isochromen-1-one (3c).** White solid; yield: 102 mg (85%); mp = 125–127 °C (lit. mp = 127–130 °C); <sup>1</sup>H NMR (CDCl<sub>3</sub>, 400 MHz) δ: 8.34 (d, *J* = 8.00 Hz, 1H), 7.92–7.89 (m, 2H), 7.78–7.73 (m, 1H), 7.56–7.52 (m, 2H), 7.19 (t, *J* = 8.50 Hz, 2H), 6.92 (s, 1H); <sup>13</sup>C NMR (CDCl<sub>3</sub>, 100 MHz) δ: 161.23, 152.82, 140.12, 137.42,

134.95, 129.72, 128.28, 127.37, 125.94, 116.11, 115.89, 101.59; HRMS (ESI-MS) ( $m/z$ ) calcd for  $C_{15}H_{10}FO_2$ : 241.0665; found 241.0645 (M + H)<sup>+</sup>.<sup>49</sup>

**3-Methyl-1H-isochromen-1-one (3d).** White solid; yield: 76 mg (95%); mp = 72–74 °C (lit. mp = 70–72 °C); <sup>1</sup>H NMR (CDCl<sub>3</sub>, 400 MHz)  $\delta$ : 8.21 (d,  $J$  = 8.24 Hz, 1H), 7.65–7.61 (m, 1H), 7.41 (t,  $J$  = 7.79 Hz, 1H), 7.30 (d,  $J$  = 7.79 Hz, 1H), 6.23 (s, 1H), 2.25 (s, 3H); <sup>13</sup>C NMR (CDCl<sub>3</sub>, 100 MHz)  $\delta$ : 162.99, 154.57, 137.65, 134.74, 129.53, 127.55, 124.85, 119.95, 103.53, 19.66; HRMS (ESI-MS) ( $m/z$ ) calcd for  $C_{10}H_8O_2$ : 161.0603; found 161.0600 (M + H)<sup>+</sup>.<sup>42</sup>

**3-Propyl-1H-isochromen-1-one (3e).** Pale yellow viscous liquid; yield: 88 mg (94%); <sup>1</sup>H NMR (CDCl<sub>3</sub>, 400 MHz)  $\delta$ : 8.28 (d,  $J$  = 8.00 Hz, 1H), 7.71–7.67 (m, 1H), 7.47 (t,  $J$  = 7.25 Hz, 1H), 7.38 (d,  $J$  = 8.00 Hz, 1H), 6.28 (s, 1H), 2.53 (t,  $J$  = 7.50 Hz, 2H), 1.82–1.72 (m, 2H), 1.02 (t,  $J$  = 7.50 Hz, 3H); <sup>13</sup>C NMR (CDCl<sub>3</sub>, 100 MHz)  $\delta$ : 163.12, 158.06, 137.62, 134.69, 129.51, 127.55, 125.00, 120.15, 103.02, 35.45, 20.24, 13.50; HRMS (ESI-MS) ( $m/z$ ) calcd for  $C_{12}H_{13}O_2$ : 189.0916; found 189.0900 (M + H)<sup>+</sup>.<sup>49</sup>

**3-Hexyl-1H-isochromen-1-one (3f).** Yellow solid; yield: 104 mg (90%); mp = 122–124 °C (lit. mp = 122–125 °C); <sup>1</sup>H NMR (CDCl<sub>3</sub>, 400 MHz)  $\delta$ : 8.26 (d,  $J$  = 7.75 Hz, 1H), 7.70–7.66 (m, 1H), 7.46 (t,  $J$  = 7.25 Hz, 1H), 7.37 (d,  $J$  = 7.75 Hz, 1H), 6.27 (s, 1H), 2.54 (t,  $J$  = 7.50 Hz, 2H), 1.76–1.68 (m, 2H), 1.44–1.27 (m, 6H), 0.91 (t,  $J$  = 6.75 Hz, 3H); <sup>13</sup>C NMR (CDCl<sub>3</sub>, 100 MHz)  $\delta$ : 163.12, 158.34, 137.65, 134.68, 129.49, 127.51, 125.01, 120.12, 102.85, 33.54, 31.51, 28.69, 26.87, 22.52, 14.04; HRMS (ESI-MS) ( $m/z$ ) calcd for  $C_{15}H_{19}O_2$ : 231.1385; found 231.1389 (M + H)<sup>+</sup>.<sup>49</sup>

**3-(Methoxymethyl)-1H-isochromen-1-one (3g).** Pale yellow solid; yield: 78 mg (82%); mp = 50–52 °C (lit. mp = 48–50 °C); <sup>1</sup>H NMR (CDCl<sub>3</sub>, 400 MHz)  $\delta$ : 8.29 (d,  $J$  = 7.75 Hz, 1H), 7.73 (t,  $J$  = 7.50 Hz, 1H), 7.53 (t,  $J$  = 7.50 Hz, 1H), 7.44 (d,  $J$  = 7.75 Hz, 1H), 6.56 (s, 1H), 4.31 (s, 2H), 3.52 (s, 3H); <sup>13</sup>C NMR (CDCl<sub>3</sub>, 100 MHz)  $\delta$ : 162.27, 153.63, 136.82, 134.89, 129.69, 128.33, 125.65, 120.72, 103.81, 70.54, 59.06; HRMS (ESI-MS) ( $m/z$ ) calcd for  $C_{11}H_{11}O_3$ : 191.0708; found 191.0712 (M + H)<sup>+</sup>.<sup>49</sup>

**4-(1-Oxo-1H-isochromen-3-yl)butanenitrile (3h).** Yellow viscous liquid; yield: 85 mg (80%); <sup>1</sup>H NMR (CDCl<sub>3</sub>, 400 MHz)  $\delta$ : 8.28 (d,  $J$  = 8.00 Hz, 1H), 7.73 (t,  $J$  = 7.75 Hz, 1H), 7.52 (t,  $J$  = 8.00 Hz, 1H), 7.41 (d,  $J$  = 8.00 Hz, 1H), 6.39 (s, 1H), 2.75 (t,  $J$  = 7.38 Hz, 2H), 2.47 (t,  $J$  = 7.00 Hz, 2H), 2.16–2.09 (m, 2H); <sup>13</sup>C NMR (CDCl<sub>3</sub>, 100 MHz)  $\delta$ : 162.57, 154.92, 136.99, 134.98, 129.64, 128.19, 125.30, 120.29, 118.84, 104.48, 32.14, 22.64, 16.41; HRMS (ESI-MS) ( $m/z$ ) calcd for  $C_{13}H_{12}NO_2$ : 214.0868; found 214.0866 (M + H)<sup>+</sup>.<sup>38</sup>

**3-Cyclopropyl-1H-isochromen-1-one (3i).** Pale yellow viscous liquid; yield: 73 mg (78%); <sup>1</sup>H NMR (CDCl<sub>3</sub>, 400 MHz)  $\delta$ : 8.20 (d,  $J$  = 7.97 Hz, 1H), 7.66–7.61 (m, 1H), 7.41–7.37 (m, 1H), 7.31 (d,  $J$  = 7.97 Hz, 1H), 6.29 (s, 1H), 1.83–1.76 (m, 1H), 1.08–1.04 (m, 2H), 0.94–0.89 (m, 2H); <sup>13</sup>C NMR (CDCl<sub>3</sub>, 100 MHz)  $\delta$ : 162.75, 158.40, 134.74, 129.55, 127.09, 124.59, 119.93, 101.37, 14.13, 13.81, 6.97; HRMS (ESI-MS) ( $m/z$ ) calcd for  $C_{12}H_{11}O_2$ : 187.0759; found 187.0751 (M + H)<sup>+</sup>.<sup>49</sup>

**3,7-Dimethyl-1H-isochromen-1-one (3j).** White solid; yield: 78 mg (90%); mp = 120–122 °C (lit. mp = 122–124 °C); <sup>1</sup>H NMR (CDCl<sub>3</sub>, 400 MHz)  $\delta$ : 8.00 (s, 1H), 7.45–7.43 (m, 1H), 7.19 (d,  $J$  = 7.79 Hz, 1H), 6.19 (s, 1H), 2.40 (s, 3H), 2.22 (s, 3H); <sup>13</sup>C NMR (CDCl<sub>3</sub>, 100 MHz)  $\delta$ : 153.65, 137.73, 136.06, 135.20, 129.21, 124.79, 119.79, 103.42, 21.34, 19.61;

HRMS (ESI-MS) ( $m/z$ ) calcd for  $C_{11}H_{11}O_2$ : 175.0759; found 175.0738 (M + H)<sup>+</sup>.<sup>42</sup>

**7-Methyl-3-phenyl-1H-isochromen-1-one (3k).** Yellow solid; yield: 103 mg (87%); mp = 95–97 °C (lit. mp = 95–96 °C); <sup>1</sup>H NMR (CDCl<sub>3</sub>, 400 MHz)  $\delta$ : 7.99 (s, 1H), 7.77–7.45 (m, 2H), 7.42–7.27 (m, 5H), 6.79 (s, 1H), 2.35 (s, 3H); <sup>13</sup>C NMR (CDCl<sub>3</sub>, 100 MHz)  $\delta$ : 162.49, 152.78, 138.49, 136.17, 135.03, 132.07, 129.73, 129.34, 128.79, 125.92, 125.08, 120.41, 101.75, 21.37; HRMS (ESI-MS) ( $m/z$ ) calcd for  $C_{16}H_{13}O_2$ : 237.0916; found 237.0925 (M + H)<sup>+</sup>.<sup>43</sup>

**7-Bromo-3-methyl-1H-isochromen-1-one (3l).** White solid; yield: 94 mg (79%); mp = 183–185 °C (lit. mp = 180–182 °C); <sup>1</sup>H NMR (CDCl<sub>3</sub>, 400 MHz)  $\delta$ : 8.36 (s, 1H), 7.77–7.34 (m, 1H), 7.24–7.21 (m, 1H), 6.24 (s, 1H), 2.28 (s, 3H); <sup>13</sup>C NMR (CDCl<sub>3</sub>, 100 MHz)  $\delta$ : 161.61, 155.15, 137.80, 136.29, 132.00, 126.47, 121.29, 120.75, 102.87, 19.69; HRMS (ESI-MS) ( $m/z$ ) calcd for  $C_{10}H_8BrO_2$ : 238.9708; found 238.9701 (M + H)<sup>+</sup> and 240.9780 (MH + 2)<sup>+</sup>.<sup>48</sup>

**7-Bromo-3-phenyl-1H-isochromen-1-one (3m).** White solid; yield: 113 mg (75%); mp = 180–182 °C (lit. mp = 181–182 °C); <sup>1</sup>H NMR (CDCl<sub>3</sub>, 400 MHz)  $\delta$ : 8.43 (s, 1H), 7.89–7.79 (m, 3H), 7.45–7.26 (m, 4H), 6.92 (s, 1H); <sup>13</sup>C NMR (CDCl<sub>3</sub>, 100 MHz)  $\delta$ : 160.99, 154.14, 138.01, 136.25, 132.22, 131.61, 130.28, 128.92, 127.55, 125.29, 121.88, 121.51, 101.07; HRMS (ESI-MS) ( $m/z$ ) calcd for  $C_{15}H_{10}BrO_2$ : 300.9864; found 300.9887 (M + H)<sup>+</sup> and 302.9825 (MH + 2)<sup>+</sup>.<sup>47</sup>

**7-Methyl-5H-pyrano[4,3-*b*]pyridin-5-one (3n).** Yellow solid; yield: 63 mg (78%); mp = 104–106 °C (lit. mp = 105–106 °C); <sup>1</sup>H NMR (CDCl<sub>3</sub>, 400 MHz)  $\delta$ : 8.85–8.84 (m, 1H), 8.47–8.44 (m, 1H), 7.37–7.34 (m, 1H), 6.50 (s, 1H), 2.32 (s, 3H); <sup>13</sup>C NMR (CDCl<sub>3</sub>, 100 MHz)  $\delta$ : 162.60, 158.82, 156.07, 154.92, 137.53, 122.54, 116.19, 105.83, 19.94; HRMS (ESI-MS) ( $m/z$ ) calcd for  $C_9H_8NO_2$ : 162.0555; found 162.0532 (M + H)<sup>+</sup>.<sup>48</sup>

**7-Phenyl-5H-pyrano[4,3-*b*]pyridin-5-one (3o).** White solid; yield: 80 mg (72%); mp = 135–137 °C (lit. mp = 136–137 °C); <sup>1</sup>H NMR (CDCl<sub>3</sub>, 400 MHz)  $\delta$ : 8.94–8.93 (m, 1H), 8.56–8.53 (m, 1H), 7.93–7.90 (m, 2H), 7.51–7.48 (m, 3H), 7.44–7.41 (m, 1H), 7.23 (s, 1H); <sup>13</sup>C NMR (CDCl<sub>3</sub>, 100 MHz)  $\delta$ : 162.01, 157.31, 156.37, 155.05, 137.59, 131.33, 130.81, 128.99, 125.66, 122.87, 116.95, 103.67; HRMS (ESI-MS) ( $m/z$ ) calcd for  $C_{14}H_{10}NO_2$ : 224.0712; found 224.0716 (M + H)<sup>+</sup>.<sup>48</sup>

## ■ ASSOCIATED CONTENT

### Supporting Information

The Supporting Information is available free of charge at <https://pubs.acs.org/doi/10.1021/acsomega.3c00710>.

TEM of the recycled nanocatalyst; green chemistry metric calculations; <sup>1</sup>H NMR and <sup>13</sup>C NMR spectra of all compounds (PDF)

## ■ AUTHOR INFORMATION

### Corresponding Author

Diwan S. Rawat – Department of Chemistry, University of Delhi, Delhi 110007, India; [orcid.org/0000-0002-5473-7476](https://orcid.org/0000-0002-5473-7476); Phone: 91-11-27662683; Email: [dsrawat@chemistry.du.ac.in](mailto:dsrawat@chemistry.du.ac.in); Fax: 91-11-27667501



## Author

Manish Rawat – Department of Chemistry, University of Delhi, Delhi 110007, India

Complete contact information is available at:

<https://pubs.acs.org/10.1021/acsomega.3c00710>

## Notes

The authors declare no competing financial interest.

## ACKNOWLEDGMENTS

D.S.R. thanks the Institute of Eminence, University of Delhi for the research grant under the FRP scheme. M.R. acknowledges CSIR for the award of Shyama Prasad Mukherjee Fellowship (file no. SPM-09/045(0249)/2016-EMR-I). We thank USIC-CIF, University of Delhi, for assistance in acquiring analytical data.

## REFERENCES

- (1) Davis, M. E. Ordered porous materials for emerging applications. *Nature* **2002**, *417*, 813–821.
- (2) White, R. J.; Luque, R.; Budarin, V. L.; Clark, J. H.; Macquarrie, D. J. Supported metal nanoparticles on porous materials. Methods and applications. *Chem. Soc. Rev.* **2009**, *38*, 481–494.
- (3) Fu, Z.; Zhang, G.; Tang, Z.; Zhang, H. Preparation and application of ordered mesoporous metal oxide catalytic materials. *Catal. Surv. Asia* **2020**, *24*, 38–58.
- (4) Corma, A. From microporous to mesoporous molecular sieve materials and their use in catalysis. *Chem. Rev.* **1997**, *97*, 2373–2420.
- (5) Ciesla, U.; Schüth, F. Ordered mesoporous materials. Microporous and mesoporous materials. *Microporous Mesoporous Mater.* **1999**, *27*, 131–149.
- (6) Ying, J. Y.; Mehnert, C. P.; Wong, M. S. Synthesis and applications of supramolecular-templated mesoporous materials. *Angew. Chem., Int. Ed.* **1999**, *38*, 56–77.
- (7) Asefa, T.; Tao, Z. Biocompatibility of mesoporous silica nanoparticles. *Chem. Res. Toxicol.* **2012**, *25*, 2265–2284.
- (8) Taguchi, A.; Schüth, F. Ordered mesoporous materials in catalysis. *Microporous Mesoporous Mater.* **2005**, *77*, 1–45.
- (9) Wang, D.; Duan, Y.; Luo, Q.; Li, X.; An, J.; Bao, L.; Shi, L. Novel preparation method for a new visible light photocatalyst: mesoporous TiO<sub>2</sub> supported Ag/AgBr. *J. Mater. Chem.* **2012**, *22*, 4847–4854.
- (10) Hackett, S. F.; Brydson, R. M.; Gass, M. H.; Harvey, I.; Newman, A. D.; Wilson, K.; Lee, A. F. High-activity, single-site mesoporous Pd/Al<sub>2</sub>O<sub>3</sub> catalysts for selective aerobic oxidation of allylic alcohols. *Am. Ethnol.* **2007**, *119*, 8747–8750.
- (11) Yuranov, I.; Moeckli, P.; Suvorova, E.; Buffat, P.; Kiwi-Minsker, L.; Renken, A. Pd/SiO<sub>2</sub> catalysts: synthesis of Pd nanoparticles with the controlled size in mesoporous silicas. *J. Mol. Catal. A: Chem.* **2003**, *192*, 239–251.
- (12) Velu, S.; Kapoor, M. P.; Inagaki, S.; Suzuki, K. Vapor phase hydrogenation of phenol over palladium supported on mesoporous CeO<sub>2</sub> and ZrO<sub>2</sub>. *Appl. Catal., A* **2003**, *245*, 317–331.
- (13) Cao, J. L.; Wang, Y.; Yu, X. L.; Wang, S. R.; Wu, S. H.; Yuan, Z. Y. Mesoporous CuO–Fe<sub>2</sub>O<sub>3</sub> composite catalysts for low-temperature carbon monoxide oxidation. *Appl. Catal., B* **2008**, *79*, 26–34.
- (14) Yang, X.; Wang, Y.; Li, M.; Sun, B.; Li, Y.; Wang, Y. Enhanced hydrogen production by steam reforming of acetic acid over a Ni catalyst supported on mesoporous MgO. *Energy Fuels* **2016**, *30*, 2198–2203.
- (15) Wu, X.; Cao, H.; Yin, G.; Yin, J.; Lu, Y.; Li, B. MgCO<sub>3</sub>·3H<sub>2</sub>O and MgO complex nanostructures: controllable biomimetic fabrication and physical chemical properties. *Phys. Chem. Chem. Phys.* **2011**, *13*, 5047–5052.
- (16) Pilarska, A. A.; Klapiszewski, L.; Jesionowski, T. Recent development in the synthesis, modification and application of Mg(OH)<sub>2</sub> and MgO: A review. *Powder Technol.* **2017**, *319*, 373–407.
- (17) Sutradhar, N.; Sinhamahapatra, A.; Roy, B.; Bajaj, H. C.; Mukhopadhyay, I.; Panda, A. B. Preparation of MgO nano-rods with strong catalytic activity via hydrated basic magnesium carbonates. *Mater. Res. Bull.* **2011**, *46*, 2163–2167.
- (18) Layek, K.; Kantam, M. L.; Shirai, M.; Nishio-Hamane, D.; Sasaki, T.; Maheswaran, H. Gold nanoparticles stabilized on nanocrystalline magnesium oxide as an active catalyst for reduction of nitroarenes in aqueous medium at room temperature. *Green Chem.* **2012**, *14*, 3164–3174.
- (19) Lemonidou, A. A.; Machli, M. Oxidative dehydrogenation of propane over V<sub>2</sub>O<sub>5</sub>-MgO/TiO<sub>2</sub> catalyst: Effect of reactants contact mode. *Catal. Today* **2007**, *127*, 132–138.
- (20) Hua, W.; Jin, L.; He, X.; Liu, J.; Hu, H. Preparation of Ni/MgO catalyst for CO<sub>2</sub> reforming of methane by dielectric-barrier discharge plasma. *Catal. Commun.* **2010**, *11*, 968–972.
- (21) Gawande, M. B.; Goswami, A.; Felpin, F. X.; Asefa, T.; Huang, X.; Silva, R.; Zou, X.; Zboril, R.; Varma, R. S. Cu and Cu-based nanoparticles: synthesis and applications in catalysis. *Chem. Rev.* **2016**, *116*, 3722–3811.
- (22) Allen, S. E.; Walvoord, R. R.; Padilla-Salinas, R.; Kozlowski, M. C. Aerobic copper-catalyzed organic reactions. *Chem. Rev.* **2013**, *113*, 6234–6458.
- (23) Aiken, J. D., III; Finke, R. G. A review of modern transition-metal nanoclusters: their synthesis, characterization, and applications in catalysis. *J. Mol. Catal. A: Chem.* **1999**, *145*, 1–44.
- (24) Verma, N.; Kumar, N. Synthesis and biomedical applications of copper oxide nanoparticles: an expanding horizon. *ACS Biomater. Sci. Eng.* **2019**, *5*, 1170–1188.
- (25) Barry, R. D. Isocoumarins Developments since 1950. *Chem. Rev.* **1964**, *64*, 229–260.
- (26) Yoshikawa, M.; Harada, E.; Naitoh, Y.; Inoue, K.; Matsuda, H.; Shimoda, H.; Yamahara, J.; Murakami, N. Development of bioactive functions in Hydrangeae Dulcis Folium. III. On the anti-allergic and antimicrobial principles of Hydrangeae Dulcis Folium (1) Thunbergins A, B, and F. *Chem. Pharm. Bull.* **1994**, *42*, 2225–2230.
- (27) Sudarshan, K.; Manna, M. K.; Aidhen, I. S. Synthesis of 3-Arylisocoumarins by Using Acyl Anion Chemistry and Synthesis of Thunbergin A and Cajanolactone A. *Eur. J. Org. Chem.* **2015**, *2015*, 1797–1803.
- (28) Kalinova, B.; Kindl, J.; Jiros, P.; Zacek, P.; Vasickova, S.; Budesinsky, M.; Valterova, I. J. Composition and electrophysiological activity of constituents identified in male wing gland secretion of the bumblebee parasite *Aphomia sociella*. *Nat. Prod.* **2009**, *72*, 8–13.
- (29) Kornsakulkarn, J.; Thongpanchang, C.; Lapanun, S.; Srichomthong, K. Isocoumarin glucosides from the scale insect fungus *Torrubiella tenuis* BCC 12732. *J. Nat. Prod.* **2009**, *72*, 1341–1343.
- (30) Shikishima, Y.; Takaishi, Y.; Honda, G.; Ito, M.; Takeda, Y.; Kodzhimatov, O. K.; Ashurmetov, O.; Lee, K. H. Chemical constituents of *Prangos tschimganica*; structure elucidation and absolute configuration of coumarin and furanocoumarin derivatives with anti-HIV activity. *Chem. Pharm. Bull.* **2001**, *49*, 877–880.
- (31) Zhang, H.; Matsuda, H.; Kumahara, A.; Ito, Y.; Nakamura, S.; Yoshikawa, M. New type of anti-diabetic compounds from the processed leaves of *Hydrangea macrophylla* var. *thunbergii* (*Hydrangeae Dulcis Folium*). *Bioorg. Med. Chem. Lett.* **2007**, *17*, 4972–4976.
- (32) Riveiro, M. E.; Moglioni, A.; Vazquez, R.; Gomez, N.; Facorro, G.; Piehl, L.; De Celis, E. R.; Shayo, C.; Davio, C. Structural insights into hydroxycoumarin-induced apoptosis in U-937 cells. *Bioorg. Med. Chem.* **2008**, *16*, 2665–2675.
- (33) Furuta, T.; Fukuyama, Y.; Asakawa, Y. Polygonolide, an isocoumarin from *Polygonum hydropiper* possessing anti-inflammatory activity. *Phytochemistry* **1986**, *25*, 517–520.
- (34) Pal, S.; Chatare, V.; Pal, M. Isocoumarin and its derivatives: An overview on their synthesis and applications. *Curr. Org. Chem.* **2011**, *15*, 782–800.
- (35) Conda-Sheridan, M.; Park, E. J.; Beck, D. E.; Reddy, P. V. N.; Nguyen, T. X.; Hu, B. J.; Chen, L.; White, J. J.; van Breemen, R. B.;

Pezzuto, J. M.; Cushman, M. Design, synthesis, and biological evaluation of indenoisoquinoline rexinoids with chemopreventive potential. *J. Med. Chem.* **2013**, *56*, 2581–2605.

(36) Dasaradhan, C.; Kumar, Y. S.; Khan, F. R. N.; Jeong, E. D.; Chung, E. H. Efficient copper-free Pd(OAc)<sub>2</sub>/Ruphos-catalyzed Sonogashira coupling in the preparation of 3'-hydroxycorfin and gymnopalynes A analogues. *Tetrahedron Lett.* **2015**, *56*, 187–191.

(37) Li, W.; Wiesenfeldt, M. P.; Glorius, F. Ruthenium–NHC–diamine catalyzed enantioselective hydrogenation of isocoumarins. *J. Am. Chem. Soc.* **2017**, *139*, 2585–2588.

(38) Korte, D. E.; Hegedus, L. S.; Wirth, R. K. Synthesis of isocoumarins, dihydroisocoumarins, and isoquinolones via pi-allylnickel halide and pi-olefin-palladium complexes. *J. Org. Chem.* **1977**, *42*, 1329–1336.

(39) Potts, K. T.; Horwitz, C. P.; Fessak, A.; Keshavarz, K. M.; Nash, K. E.; Toscano, P. J. Coordination of ethynylpyridine ligands with copper (I): x-ray structure of a novel triple-helical, tricuprous complex. *J. Am. Chem. Soc.* **1993**, *115*, 10444–10445.

(40) Novak, Z.; Szabo, A.; Repasi, J.; Kotschy, A. Sonogashira coupling of aryl halides catalyzed by palladium on charcoal. *J. Org. Chem.* **2003**, *68*, 3327–3329.

(41) Ueura, K.; Satoh, T.; Miura, M. Rhodium- and iridium-catalyzed oxidative coupling of benzoic acids with alkynes via regioselective C–H bond cleavage. *J. Org. Chem.* **2007**, *72*, 5362–5367.

(42) Kavala, V.; Wang, C. C.; Barange, D. K.; Kuo, C. W.; Lei, P. M.; Yao, C. F. Synthesis of isocoumarin derivatives via the copper-catalyzed tandem sequential cyclization of 2-halo-N-phenyl benzamides and acyclic 1,3-diketones. *J. Org. Chem.* **2012**, *77*, S022–S029.

(43) Jiang, G.; Li, J.; Zhu, C.; Wu, W.; Jiang, H. Palladium-catalyzed sequential nucleophilic addition/oxidative annulation of bromoalkynes with benzoic acids to construct functionalized isocoumarins. *Org. Lett.* **2017**, *19*, 4440–4443.

(44) Kumar, M. R.; Irudayanathan, F. M.; Moon, J. H.; Lee, S. Regioselective one-pot synthesis of isocoumarins and phthalides from 2-iodobenzoic acids and alkynes by temperature control. *Adv. Synth. Catal.* **2013**, *355*, 3221–3230.

(45) Gianni, J.; Pirovano, V.; Abbiati, G. Silver triflate/p-TSA cocatalyzed synthesis of 3-substituted isocoumarins from 2-alkynylbenzoates. *Org. Biomol. Chem.* **2018**, *16*, 3213–3219.

(46) Subramanian, V.; Batchu, V. R.; Barange, D.; Pal, M. Synthesis of isocoumarins via Pd/C-mediated reactions of o-iodobenzoic acid with terminal alkynes. *J. Org. Chem.* **2005**, *70*, 4778–4783.

(47) Sun, M.; Su, L.; Dong, J.; Liu, L.; Zhou, Y.; Yin, S. F. Copper-catalyzed annulation of 2-bromobenzoic esters with terminal alkynes towards 3-substituted isocoumarins. *Tetrahedron Lett.* **2017**, *58*, 2433–2437.

(48) Hellal, M.; Bourguignon, J. J.; Bihel, F. J. J. 6-endo-dig cyclization of heteroarylesters to alkynes promoted by Lewis acid catalyst in the presence of Brønsted acid. *Tetrahedron Lett.* **2008**, *49*, 62–65.

(49) Chary, R. G.; Reddy, G. R.; Ganesh, Y. S. S.; Prasad, K. V.; Chandra, S. P.; Mukherjee, S.; Pal, M. Cu-catalyzed coupling-cyclization in PEG 400 under ultrasound: a highly selective and greener approach towards isocoumarins. *RSC Adv.* **2013**, *3*, 9641–9644.

(50) Rawat, M.; Rawat, D. S. CuO@NiO nanocomposite catalyzed synthesis of biologically active indenoisoquinoline derivatives. *ACS Sustainable Chem. Eng.* **2020**, *8*, 13701–13712.

(51) Purohit, G.; Kharkwal, A.; Rawat, D. S. CuIn-ethylxanthate, a “Versatile Precursor” for photosensitization of graphene-quantum dots and nanocatalyzed synthesis of imidazopyridines with ideal green chemistry metrics. *ACS Sustainable Chem. Eng.* **2020**, *8*, 5544–5557.

(52) Rawat, M.; Rawat, D. S. Cu<sub>2</sub>O-decorated marigold hollow alumina microsphere nanoparticles as a robust and efficient catalyst for the synthesis of isoquinolones. *ACS Sustainable Chem. Eng.* **2022**, *10*, 10014–10023.

(53) Rawat, M.; Rawat, D. S. Copper oxide nanoparticle catalyzed synthesis of imidazo [1, 2-a] pyrimidine derivatives, their optical

properties and selective fluorescent sensor towards zinc ion. *Tetrahedron Lett.* **2018**, *59*, 2341–2346.

(54) Liu, S.; Wang, Z.; Han, T.; Fei, T.; Zhang, T. Mesoporous magnesium oxide nanosheet electrocatalysts for the detection of Lead (II). *ACS Appl. Nano Mater.* **2019**, *2*, 2606–2611.

(55) Wang, C.; Higgins, D.; Wang, F. F.; Li, D. Y.; Liu, R. Q.; Xia, G. F.; Li, N.; Li, Q.; Xu, H.; Wu, G. Controlled synthesis of micro/nanostructured CuO anodes for lithium-ion batteries. *Nano Energy* **2014**, *9*, 334–344.

(56) Yang, S.; Huang, P.; Peng, L.; Cao, C.; Zhu, Y.; Wei, F.; Sun, Y.; Song, W. Hierarchical flowerlike magnesium oxide hollow spheres with extremely high surface area for adsorption and catalysis. *J. Mater. Chem. A* **2016**, *4*, 400–406.

(57) Hashim, K. S.; Al-Saati, N. H.; Hussein, A. H.; Al-Saati, Z. N. An investigation into the level of heavy metals leaching from canal-dredged sediment: A case study metals leaching from dredged sediment. *IOP Conf. Ser.: Mater. Sci. Eng.* **2018**, *454*, No. 012022.